Inorganic Chemistry
Article

*Inorg. Chem.* **2011**, *50*, 1775–1785 **1775**
DOI: 10.1021/ic102195w

# Isomeric Complexes of [$Ru^{II}$(trpy)(L)Cl] (trpy = 2,2′:6′,2″-Terpyridine and HL = Quinaldic Acid): Preference of Isomeric Structural Form in Catalytic Chemoselective Epoxidation Process

**Abhishek Dutta Chowdhury, Amit Das, Irshad K, Shaikh M. Mobin, and Goutam Kumar Lahiri***

*Department of Chemistry, Indian Institute of Technology Bombay, Powai, Mumbai-400076, India*

Received November 1, 2010

The present work deals with the isomeric complexes of the molecular composition [$Ru^{II}$(trpy)(L)Cl] in **1** and **2** (trpy = 2,2′:6′,2″-terpyridine, L = deprotonated form of quinaldic acid, HL). Isomeric identities of **1** and **2** have been established by their single-crystal X-ray structures, which reveal that under the meridional configuration of trpy, $O^-$ and N donors of the unsymmetrical L are in *trans*, *cis* and *cis*, *trans* configurations, respectively, with respect to the Ru−Cl bond. Compounds **1** and **2** exhibit appreciable differences in bond distances involving Ru−Cl and Ru−O1/Ru−N1 associated with L on the basis of their isomeric structural features. In relation to isomer **2**, the isomeric complex **1** exhibits a slightly lower Ru(II)−Ru(III) oxidation potential [0.35 (**1**), 0.38 (**2**) V versus SCE in $CH_3CN$] as well as lower energy MLCT transitions [559 nm and 417 nm (**1**) and 533 nm and 378 nm (**2**)]. This has also been reflected in the DFT calculation where a lower HOMO−LUMO gap of 2.59 eV in **1** compared to 2.71 eV in **2** is found. The isomeric structural effect in **1** and **2** has also been prominent in their $^1H$ NMR spectral profiles. The relatively longer Ru−Cl bond in **1** (2.408(2) Å) as compared to **2** (2.3813(9) Å) due to the *trans* effect of the anionic $O^-$ of coordinated L makes it labile, which in turn facilitates the transformation of [$Ru^{II}$(trpy)(L)(Cl)] (**1**) to the solvate species, [$Ru^{II}$(trpy)(L)($CH_3CN$)](Cl) (**1a**) while crystallizing **1** from the coordinating $CH_3CN$ solvent. The formation of **1a** has been authenticated by its single-crystal X-ray structure. However, no such exchange of "$Cl^-$" by the solvent molecule occurs in **2** during the crystallization process from the coordinating $CH_3CN$ solvent. The labile Ru−Cl bond in **1** makes it a much superior precatalyst for the epoxidation of alkene functionalities. Compound **1** is found to function as an excellent precatalyst for the epoxidation of a wide variety of alkene functionalities under environmentally benign conditions using $H_2O_2$ as an oxidant and EtOH as a solvent, while isomer **2** remains almost ineffective under identical reaction conditions. The remarkable differences in catalytic performances of **1** and **2** based on their isomeric structural aspects have been addressed.

## Introduction

Metal complex catalyzed epoxidation of alkenes is known to be an industrially important and synthetically challenging chemical process.[1−3] Traditionally, epoxidation of alkenes can be performed using various organic peracids as oxidants without the involvement of metal ions, but it has severe limitations, particularly from the point of view of generating a large quantity of organic waste, narrow substrate scope, and inconvenience in separating the products.[2] However, early transition metal complexes have subsequently been established as efficient catalysts for the epoxidation reaction in combination with a wide variety of oxidants.[3] On the contrary, ruthenium catalyzed epoxidation reaction is rather limited to a few selective molecular frameworks.[4,5] Ruthenium

*To whom correspondence should be addressed. E-mail: lahiri@chem.iitb.ac.in.

(1) (a) Barf, G. A.; Sheldon, R. A. *J. Mol. Catal. A: Chem.* **1995**, *102*, 23 and references cited therein. (b) Sheldon, R. A.; Kochi, J. K. *Metal-Catalyzed Oxidations of Organic Compounds*; Academic Press: New York, 1981. (c) Bäckvall; J.-E. *Modern Oxidation Methods*; Wiley-VCH: Weinheim, Germany, 2004. (d) Sheldon, R. A.; Arends, I.; Hanefeld, U. *Green Chemistry and Catalysis*; Wiley-VCH: Weinheim, Germany, 2007. (e) Weissermel, K.; Arpe, H.-J. *Industrial Organic Chemistry*, 4th ed.; Wiley-VCH: Weinheim, Germany, 2003.

(2) (a) Crawford, K.; Rautenstrauch, V.; Uijttewaal, A. *Synlett* **2001**, 1127. (b) Wahren, U.; Sprung, I.; Schulze, K.; Findeisen, M.; Buchbauer, G. *Tetrahedron Lett.* **1999**, *40*, 5991. (c) Kelly, D. R.; Nally, J. *Tetrahedron Lett.* **1999**, *40*, 3251.

(3) (a) Grigoropoulou, G.; Clark, J. H.; Elings, J. A. *Green Chem.* **2003**, *5*, 1. (b) Lane, B. S.; Burgess, K. *Chem. Rev.* **2003**, *103*, 2457. (c) Beller, M. *Adv. Synth. Catal.* **2004**, *346*, 107. (d) Legros, J.; Bolm, C. *Chem.—Eur. J.* **2005**, *11*, 1086. (e) Bregeault, J. M. *Dalton Trans.* **2003**, 3289. (f) Herrmann, W. A.; Fischer, R. W.; Marz, D. W. *Angew. Chem., Int. Ed.* **1991**, *30*, 1638. (g) Rudolf, J.; Reddy, K. L.; Chiang, J. P.; Sharpless, K. B. *J. Am. Chem. Soc.* **1997**, *119*, 6189. (h) Hermann, W. A.; Kratzer, R. M.; Ding, H.; Thiel, W. R.; Glas, H. *J. Organomet. Chem.* **1998**, *555*, 293. (i) Shi, Y. *Acc. Chem. Res.* **2004**, *37*, 488. (j) Gerlach, A.; Geller, T. *Adv. Synth. Catal.* **2004**, *346*, 1247. (k) Yang, D. *Acc. Chem. Res.* **2004**, *37*, 497. (l) Johnson, R. A.; Sharpless, K. B. *Catalytic Asymmetric Synthesis*; Ojima, I., Ed.; VCH: New York, 1993; Chapter 4.1. (m) Katsuki, T.; Martin, V. S. *Org. React.* **1996**, *48*, 1. (n) Jacobsen, E. N. *Catalytic Asymmetric Synthesis*; Ojima, I., Ed.; VCH: New York, 1993; Chapter 4.2. (o) Katsuki, T. *Adv. Synth. Catal.* **2002**, *344*, 131. (p) Cavallo, L.; Jacobsen, H. *Angew. Chem., Int. Ed.* **2000**, *39*, 589.


Published on Web 01/18/2011

complex derived effective expoxidation catalyst [$Ru^{II}$(trpy)-(dipic)] (trpy = 2,2′:6′,2″-terpyridine, dipic = 2,6-pyridinedicarboxylic acid) was first reported by Nishiyama et al. in 1997,[4a] and only recently has a significant expansion of the scope of ruthenium based catalysts toward the epoxidation reactions been made by Beller et al.[5] It is now well recognized that ruthenium complexes of polypyridine or pybox (pybox = pyridine bis(oxazoline)) or Schiff-based derived ligands are suitable precatalysts for the epoxidation of various alkene functionalities using different oxidants such as hydrogen peroxide, organic peracids, etc.[4,5] It should be noted that ruthenium complexes were earlier considered to decompose $H_2O_2$ instead of activating $H_2O_2$ to form the active {Ru=O} state, but Beller et al. have shown recently that $H_2O_2$ can also be a good oxidant for the ruthenium catalyzed epoxidation process.[5d]

The present work is therefore specifically originated from the following perspectives: (i) designing isomeric ruthenium-polypyridyl derivatives, [$Ru^{II}$(trpy)(L)Cl] (**1** and **2**), under the meridionally coordinated trpy (trpy = 2,2′:6′,2″-terpyridine) in combination with a deprotonated form of unsymmetrical quinaldic acid, HL; (ii) exploration of the potential application of isomeric **1** and **2** for the catalytic epoxidation process under environmentally benign reaction conditions; (iii) investigation of the effect of isomeric structural features in **1** and **2** on the catalytic epoxidation process.

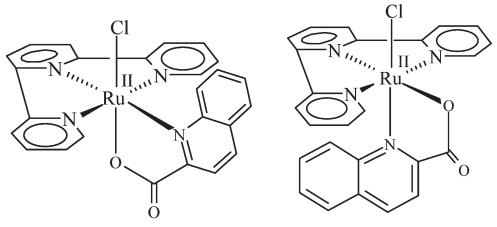

**1** **2**

Herein, we report the synthetic and structural aspects of the isomeric complexes **1** and **2** as well as the effect of isomeric structural features on their spectroscopic and electrochemical properties. The catalytic aspects of the isomeric complexes **1** and **2** have been explored toward the epoxidations of a wide variety of olefinic substrates using different oxidants and solvents. Remarkably, the isomeric form **1** with electron rich anionic "$O^-$" of L *trans* to the Ru−Cl bond exhibits superior epoxidation activity as compared to the isomeric form **2** with neutral "N" of L *trans* to the Ru−Cl bond. The origin of the difference in catalytic performances primarily based on the isomeric structural features of **1** and **2** has been investigated experimentally and using DFT calculations. To the best of our knowledge, the present work demonstrates for the first time the significant effect of isomeric structures as in **1** and **2** on the catalytic epoxidation process.

## Results and Discussion

**Synthesis and Structural Aspects of Isomeric Complexes 1 and 2.** The isomeric complexes of molecular composition [$Ru^{II}$(trpy)(L)Cl] (trpy = 2,2′:6′,2″-terpyridine, L = deprotonated form of unsymmetrical quinaldic acid, HL), **1** ($O^-$ of L *trans* to $Cl^-$) and **2** (N of L *trans* to $Cl^-$), have been prepared via the reaction of $Ru^{III}(trpy)Cl_3$ with HL in the presence of $NEt_3$ as a base in EtOH under a dinitrogen atmosphere. The isomers **1** (blue-violet) and **2** (red-violet) have been separated using a neutral alumina column (see the Experimental Section). The electrically neutral and diamagnetic **1** and **2** are stable and resistant to any interconversion in both the solid and solution states. The DFT calculations based on the optimized structures of **1** and **2** (Figure S1 in the Supporting Information (SI)) at the B3LYP level predict that isomer **1** is slightly more stable (5.6 kcal/mol) compared to isomer **2**.

The isomeric features of **1** and **2** have been authenticated by their single-crystal X-ray structures (Figure 1, Table 1, and Table S1 in the SI). The bidentate L is bonded to the ruthenium(II) ion *via* the O1$^-$ and N1 donors forming a five-membered chelate ring.[6] Under the usual meridional configuration of trpy,[7] the $O^-$ and N donors of the unsymmetrical bidentate L are in *trans*, *cis* and *cis*, *trans* configurations in relation to the sixth monodentate chloride ligand in **1** and **2**, respectively. The bond distances and angles in **1** and **2** (Table S1 in the SI) are in good agreement with the reported data of analogous complexes.[6,7] The geometrical constraints due to the meridional mode of trpy[7] have been reflected in the appreciably smaller *trans* angle involving the trpy ligand, N2−Ru−N4 at 159.6(3)° and 160.97(12)° in **1** and **2**, respectively. The central Ru−N3(trpy) bond lengths of 1.934(7) and 1.925(3) Å in **1** and **2**, respectively, are significantly shorter than the corresponding distances involving the terminal pyridine

(4) (a) Nishiyama, H.; Shimada, T.; Itoh, H.; Sugiyama, H.; Motoyama, Y. *Chem. Commun.* **1997**, 1863. (b) End, N.; Pfaltz, A. *Chem. Commun.* **1998**, 589. (c) Gross, Z.; Ini, S. *Org. Lett.* **1999**, *1*, 2077 and references therein. (d) Stoop, R. M.; Bachmann, S.; Valentini, M.; Mezzetti, A. *Organometallics* **2000**, *19*, 4117. (e) Pezet, F.; Aït-Haddou, H.; Daran, J.-C.; Sadaki, I.; Balavoine, G. G. A. *Chem. Commun.* **2002**, 510. (f) Takeda, T.; Irie, R.; Shinoda, Y.; Katsuki, T. *Synlett* **1999**, 1157. (g) Nakata, K.; Takeda, T.; Mihara, J.; Hamada, T.; Irie, R.; Katsuki, T. *Chem.—Eur. J.* **2001**, *7*, 3776. (h) Dakkach, M.; Isabel López, M.; Romero, I.; Rodríguez, M.; Atlamsani, A.; Parella, T.; Fontrodona, X.; Llobet, A. *Inorg. Chem.* **2010**, *49*, 5977. (i) Chatterjee, D. *Inorg. Chim. Acta* **2008**, *361*, 2177. (j) Chatterjee, D.; Sengupta, A.; Mitra, A. *Polyhedron* **2007**, *26*, 178. (k) Benet-Buchholz, J.; Comba, P.; Llobet, A.; Roeser, S.; Vadivelu, P.; Wadepohl, H.; Wiesner, S. *Dalton Trans.* **2009**, 5910.

(5) (a) Klawonn, M.; Tse, M. K.; Bhor, S.; Döbler, C.; Beller, M. *J. Mol. Catal. A* **2004**, *218*, 13. (b) Tse, M. K.; Bhor, S.; Klawonn, M.; Döbler, C.; Beller, M. *Tetrahedron Lett.* **2003**, *44*, 7479. (c) Bhor, S.; Tse, M. K.; Klawonn, M.; Döbler, C.; Beller, M.; Mägerlein, W. *Adv. Synth. Catal.* **2004**, *346*, 263. (d) Tse, M. K.; Döbler, C.; Bhor, S.; Klawonn, M.; Mägerlein, W.; Hugl, H.; Beller, M. *Angew. Chem., Int. Ed.* **2004**, *43*, 5255. (e) Tse, M. K.; Bhor, S.; Klawonn, M.; Anilkumar, G.; Jiao, H.; Spannenberg, S.; Döbler, C.; Mägerlein, W.; Hugl, H.; Beller, M. *Chem.—Eur. J.* **2006**, *12*, 1875. (f) Tse, M. K.; Bhor, S.; Klawonn, M.; Bhor, S.; Döbler, C.; Anilkumar, G.; Hugl, H.; Mägerlein, W.; Beller, M. *Org. Lett.* **2005**, *7*, 987. (g) Schröder, K.; Enthaler, S.; Join, B.; Junge, K.; Beller, M. *Adv. Synth. Catal.* **2010**, *352*, 1771.

(6) Kundu, T.; Sarkar, B.; Mondal, T. K.; Fiedler, J.; Mobin, S. M.; Kaim, W.; Lahiri, G. K. *Inorg. Chem.* **2010**, *49*, 6565.

(7) (a) Patra, S.; Sarkar, B.; Ghumaan, S.; Patil, M. P.; Mobin, S. M.; Sunoj, R. B.; Kaim, W.; Lahiri, G. K. *Dalton Trans.* **2005**, 1188. (b) Sarkar, S.; Sarkar, B.; Chanda, N.; Kar, S.; Mobin, S. M.; Fiedler, J.; Kaim, W.; Lahiri, G. K. *Inorg. Chem.* **2005**, *44*, 6092. (c) Chanda, N.; Paul, D.; Kar, S.; Mobin, S. M.; Datta, A.; Puranik, V. G.; Rao, K. K.; Lahiri, G. K. *Inorg. Chem.* **2005**, *44*, 3499. (d) Chanda, N.; Mobin, S. M.; Puranik, V. G.; Dutta, A.; Niemeyer, M.; Lahiri, G. K. *Inorg. Chem.* **2004**, *43*, 1056. (e) Mondal, B.; Puranik, V. G.; Lahiri, G. K. *Inorg. Chem.* **2002**, *41*, 5831. (f) De, P.; Sarkar, B.; Maji, S.; Das, A. K.; Bulak, E.; Mobin, S. M.; Kaim, W.; Lahiri, G. K. *Eur. J. Inorg. Chem.* **2009**, 2702. (g) Das, A. K.; Sarkar, B.; Duboc, C.; Strobel, S.; Fiedler, J.; Zalis, S.; Lahiri, G. K.; Kaim, W. *Angew. Chem., Int. Ed.* **2009**, *48*, 4242. (h) Sans, C.; Rodriguez, M.; Romero, I.; Llobet, A. *Inorg. Chem.* **2003**, *42*, 8385. (i) Hartshorn, C. M.; Maxwell, K. A.; White, P. S.; DeSimone, J. M.; Meyer, T. J. *Inorg. Chem.* **2001**, *40*, 601.

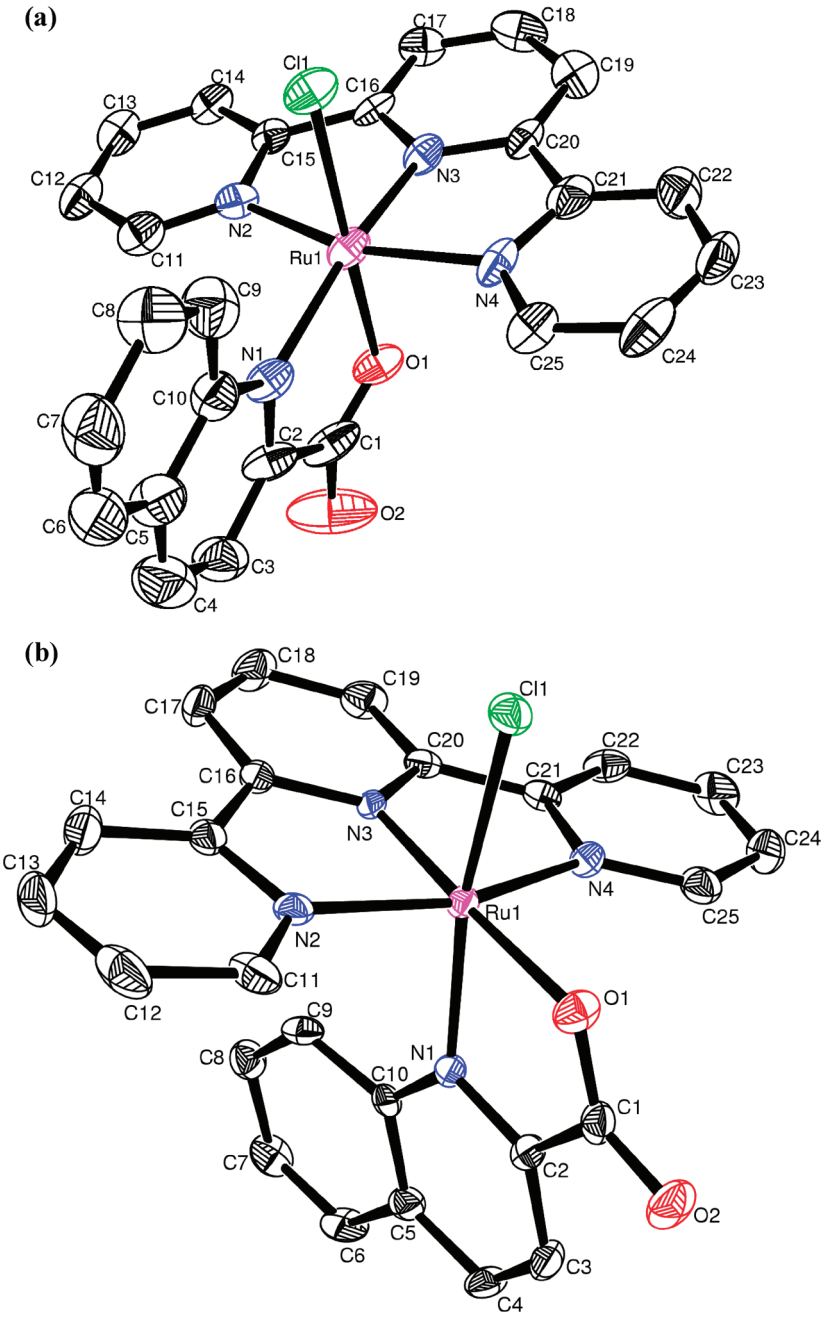


**Figure 1.** ORTEP diagrams of [Ru(trpy)(L)(Cl)]. (a) Isomer **1** and (b) Isomer **2**. Thermal ellipsoids are drawn at 50% probability. The solvents of crystallization and hydrogen atoms are omitted for clarity. Selected bond distance (Å)/bond angles (deg) of **1**: Ru−Cl, 2.408(2); Ru−N(1), 2.136(7); Ru−N(2), 2.074(7); Ru−N(3), 1.934(7); Ru−N(4), 2.049(6); Ru−O(1), 2.064(6); O(1)−Ru−N(3), 91.8(3); N(1)−Ru−N(3), 169.7(3); O(1)−Ru−Cl, 175.59(18); N(1)−Ru−Cl, 105.9(2). Selected bond distance (Å)/bond angle (deg) of **2**: Ru−Cl, 2.3813(9); Ru−N(1), 2.102(3); Ru−N(2), 2.051(3); Ru−N(3), 1.925(3); Ru−N(4), 2.045(3); Ru−O(1), 2.099(2); O(1)−Ru−N(3), 177.49(10); N(1)−Ru−N(3), 104.20(11); O(1)−Ru−Cl, 91.18(7); N(1)−Ru−Cl, 168.89(8).

rings of trpy, Ru−N2(trpy), 2.074(7) and 2.051(3) Å, and Ru−N4(trpy), 2.049(6) and 2.045(3) Å, respectively.

The Ru−Cl bond distances in isomeric **1** and **2** are 2.408(2) Å and 2.3813(9) Å, respectively.[7a] The presence of negatively charged $O^-$ of L *trans* to $Cl^-$ makes the Ru−Cl bond in **1** selectively 0.02 Å longer than that in **2**, where the neutral N of L is *trans* to $Cl^-$. This in turn makes the Ru−$O^-$(L) bond shorter in **1** (2.064(6) Å) relative to **2** (2.099(2) Å). On the other hand, the Ru−N(1)(L) distance in **2** (2.102(3) Å) is shorter than that in **1** (2.136(7) Å), primarily due to the enhanced Ru(II) → quinoline(L) back-bonding via the involvement of $\sigma$- and $\pi$-donating chloride ions *trans* to N1(L) in **2**.[6] The central Ru−N3(trpy) distance in **1** is ∼0.01 Å longer than that in **2** due to the presence of a moderately $\pi$-accepting quinoline ring of L *trans* to the strongly $\pi$-accepting N(3)(trpy) in **1**, while in **2**, the donating $O^-$ of the carboxylate anion (C(=O)$O^-$) of L is *trans* to Ru−N3(trpy). The isomers also exert appreciable differences in the *trans* angle involving (L)−Ru−Cl: O1−Ru−Cl at 175.59° in **1** versus N1−Ru−Cl at 168.89° in **2**; the bulkier quinoline ring *trans* to Ru−Cl in **2** makes it relatively bent.

The DFT calculated bond distances and angles (Table S1 in the SI) based on the optimized structures of **1** and **2**

**Table 1.** Selected Crystallographic Parameters

| | $1\cdot 0.5H_2O\cdot 2CH_2Cl_2$ | $2(\mathbf{1a})\cdot 12H_2O.CH_3CN$ | $2\cdot H_2O$ |
|---|---|---|---|
| empirical formula | $C_{27}H_{22}Cl_5N_4O_{2.5}Ru$ | $C_{56}H_{40}Cl_2N_{11}O_{16}Ru_2$ | $C_{25}H_{19}ClN_4O_3Ru$ |
| fw | 720.81 | 1396.03 | 559.96 |
| cryst syst | monoclinic | triclinic | orthorhombic |
| space group | $P21/c$ | $P1$ | $Pna21$ |
| $a$ (Å) | 8.4741(5) | 13.3237(4) | 14.5284(3) |
| $b$ (Å) | 30.782(2) | 14.4717(6) | 16.8813(4) |
| $c$ (Å) | 11.1688(9) | 18.3936(6) | 8.9158(2) |
| α (deg) | 90 | 105.741(3) | 90 |
| $\beta$ (deg) | 104.180(7) | 93.689(2) | 90 |
| $\gamma$ (deg) | 90 | 113.068(4) | 90 |
| $V$ (Å$^3$) | 2824.6(4) | 3081.78(19) | 2186.67(8) |
| $Z$ | 4 | 2 | 4 |
| $\mu$ (mm$^{-1}$) | 1.064 | 0.652 | 0.877 |
| $T$ (K) | 150(2) | 150(2) | 150(2) |
| $D_{calcd}$ (g cm$^{-3}$) | 1.695 | 1.504 | 1.701 |
| F(000) | 1444 | 1406 | 1128 |
| $\theta$ range (deg) | 3.25 to 25.00 | 3.33 to 25.00 | 3.61 to 25.00 |
| data/restraints/params | 4961/0/365 | 10827/0/786 | 3606/1/315 |
| R1, wR2 [I > 2$\sigma$(I)] | 0.0613, 0.1434 | 0.0710, 0.2078 | 0.0271, 0.0442 |
| R1, wR2 (all data) | 0.1272, 0.1556 | 0.0948, 0.2215 | 0.0362, 0.0454 |
| GOF | 0.912 | 1.037 | 0.904 |
| largest diff. peak/hole (e Å$^{-3}$) | 1.602 and −0.992 | 1.432 and −1.385 | 0.321 and −0.271 |

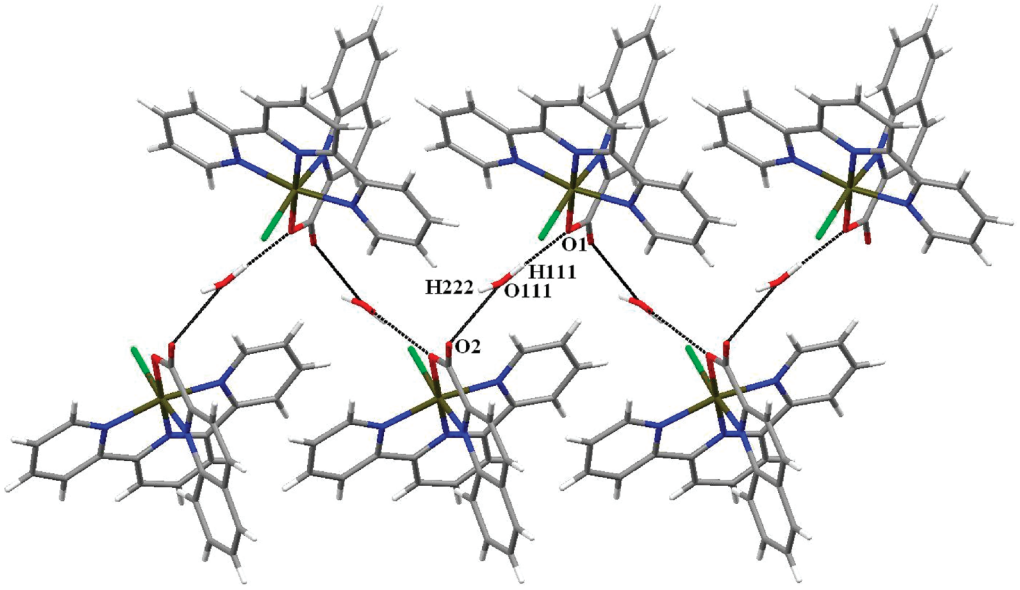


**Figure 2.** Packing diagram of **2** along the *b* axis.

(Figure S1 in the SI) are in general agreement with the X-ray data.

The packing diagram of **2** reveals the presence of strong C−H···O hydrogen bonding interactions between the hydrogen atoms (H111 and H222) of the lattice water molecule (O111) and coordinated oxygen (O1) as well as pendant oxygen (O2) atoms of the carboxylate group of L. The two hydrogen atoms of the lattice water molecule are connected to two different oxygen atoms, O1 and O2 of L associated with the adjacent two Ru complexes (**2**), leading to the formation of a 1D-zigzag chain (Figure 2, Table S2 in the SI).

**Spectral and Redox Aspects.** The $\nu$(C=O) frequency of free HL at 1700 cm$^{-1}$ [6] has been appreciably shifted on coordination to 1635 and 1629 cm$^{-1}$, as revealed by the IR spectra of **1** and **2**, respectively. $^1$H NMR spectra of **1** and **2** exhibit a calculated number of 17 partially overlapping aromatic proton resonances each in $(CD_3)_2SO$, and the extent of overlapping of proton signals is appreciably larger in **1** as compared to **2** (Figure 3 and see the Experimental Section). However, the spectra are quite distinct with respect to their isomeric identities. For example, the maximum downfield shifted signal for **1** corresponding to the proton *para* to the quinoline nitrogen (N1) of L appears at 10.2 ppm, while the same in **2** appears at 8.75 ppm.[8] This is primarily due to the *trans* orientation of the N1 of L with respect to the central pyridine ring of the $\pi$-acceptor trpy and $\sigma/\pi$-donor chloride atom in **1** and **2**, respectively. A similar ∼1 ppm difference in chemical shift due to the isomeric structural effect has also been reflected for the proton adjacent to the N(1) center but in the fused benzene ring of L, 7.5 ppm in **1** and 6.5 ppm in **2** (Figure 3).

Complexes **1** and **2** exhibit two moderately intense transitions each in the visible region, 559 and 417 nm and 533 and 378 nm, respectively, followed by several intense

(8) Zhang, H.-J.; Demerseman, B.; Toupet, L.; Xi, Z.; Bruneau, C. *Organometallics* **2009**, *28*, 5173.

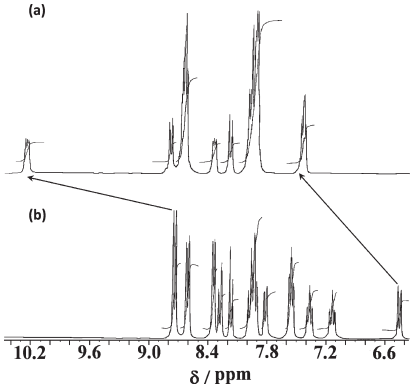


**Figure 3.** $^1$H NMR spectra of (a) **1** and (b) **2** in $(CD_3)_2SO$.

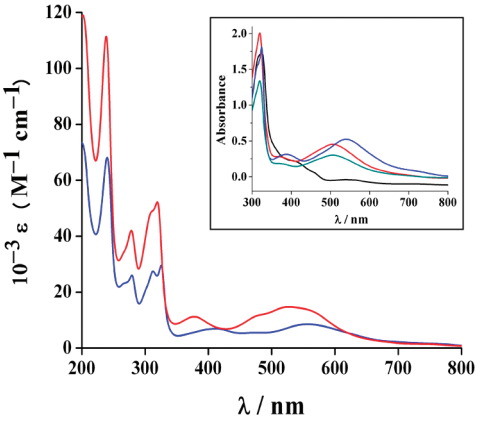


**Figure 4.** Electronic spectra of **1** (blue) and **2** (red) in $CH_3CN$. Inset: Electronic spectra of $[Ru(trpy)(L)(Cl)]$ (**1**, blue), $[Ru(trpy)(L)(EtOH)]^+$ (green), **1** in the presence of $H_2O_2$, i.e., in situ generated $[Ru(trpy)(L)(O)]^+$ (**3**, black), and **3** + $PPh_3$ (Red) in EtOH.

higher energy intraligand transitions in the UV region in $CH_3CN$ (Figure 4, see the Experimental Section).[7,9] The two visible energy bands near 550 and 400 nm are assigned on the basis of the TD-DFT calculations on the optimized structures of **1** and **2** as $d\pi(Ru^{II}) \rightarrow p\pi^*(trpy)/p\pi^*(L)$ and $d\pi(Ru^{II}) \rightarrow p\pi^*(L)$ transitions, respectively (Tables S3 and S4 in the SI). Interestingly, isomeric complexes **1** and **2** are quite distinct with respect to their lowest energy MLCT (metal-to-ligand charge transfer) band positions at 559 nm (17 889 $cm^{-1}$) and 533 nm (18 762 $cm^{-1}$), respectively. The MLCT transition energy 873 $cm^{-1}$ lower in **1** with respect to **2** has also been reflected in the HOMO−LUMO gaps of 2.59 and 2.71 eV in **1** and **2**, respectively (Figure 5). Furthermore, the intensity of the 533 nm band in **2** of $\varepsilon$ = 14 710 $M^{-1}$ $cm^{-1}$ is almost double that in **1** at 559 nm, $\varepsilon$ = 8477 $M^{-1}$ $cm^{-1}$. A similar trend in the isomer based difference in intensity of the MLCT bands has been reported in isomeric $[Ru(trpy)(3\text{-amino-}6\text{-}(3,5\text{-dimethylpyrazol-}1\text{-yl})\text{-}1,2,4,5\text{-tetrazine})(Cl)]^+$.[7a]

The orbital contributions in MOs in **1** and **2** (Figure 5 and Tables S5 and S6 in the SI) predict that the HOMOs (HOMO to HOMO−3) are primarily composed of metal-based orbitals with varying partial contributions from Cl, trpy, or L. Accordingly, reversible $Ru^{II} \rightleftharpoons Ru^{III}$ couples in **1** and **2** appear at $E_{298}$°, V ($\Delta E_p$, mV), of 0.35(70) and 0.38(65) in $CH_3CN$ versus SCE (Figure S2 in the SI). The

(9) Llobet, A.; Doppelt, P.; Meyer, T. J. *Inorg. Chem.* **1988**, *27*, 514.

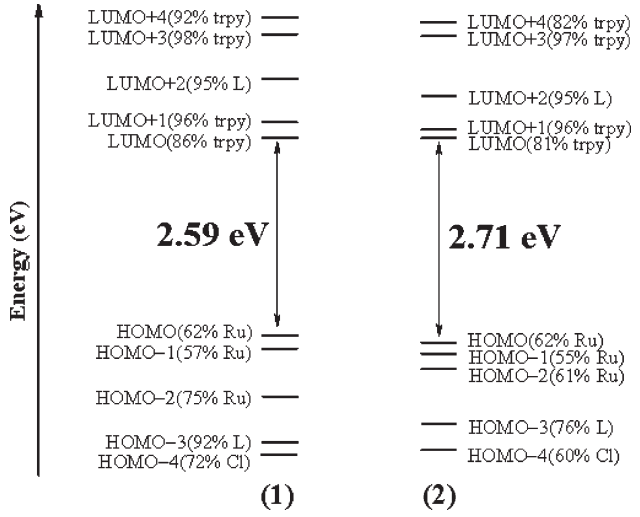


**Figure 5.** Schematic representation of MOs, showing the difference in energy gap between HOMO and LUMO in **1** and **2**.

relatively lower stability of the Ru(II) state in **1** as compared to **2** can be attributed to the greater electron density on the ruthenium ion due to the *trans* orientation of the negatively charged $O^-$(L) and $Cl^-$ in **1**, while the same in **2** are in *cis* orientation. This has also been reflected in the less positive NBO charge on Ru of 0.67 in **1** relative to 0.69 in **2** (Table S7 in the SI). A similar trend in Ru(II)/Ru(III) potential ($E_{cis}$° > $E_{trans}$°) has been reported for the analogous picolinate derivative [Ru(trpy)(picolinate)Cl].[9]

The trpy based (Figure 5 and Tables S5 and S6 in the SI) quasi-reversible reductions in **1** and **2** appear at $E_{298}$°, V ($\Delta E_p$, mV), of −0.838(100) and −1.395 (80) and of −0.902(110) and −1.54(110), respectively.[7,9]

The aforementioned difference in electronic structural aspects in **1** and **2** primarily based on their isomeric structural features has indeed instigated a look into the following: (i) the potential applications of **1** and **2** as precatalysts for the epoxidation process and (ii) their effect on catalytic performances.

**Catalytic Epoxidation Reactions.** The isomeric complexes **1** and **2** have been tested for the epoxidation of a wide variety of alkene functionalities using $H_2O_2$, $^t$BuOOH (tert-butylhydroperoxide, TBHP), and *m*-CPBA (*meta*-chloroperbenzoic acid) as possible oxidants in solvents such as $C_2H_5OH$, $CH_2Cl_2$, and $CH_3CN$ under neutral reaction conditions.[5] The catalytic results are listed in Table 2. Remarkably, isomeric complexes **1** and **2** exhibit significant differences in their catalytic performances toward the epoxidation of alkene functionalities (Table 2) primarily based on their built-in differences in structural/electronic properties (see later). Considering $H_2O_2$, TBHP, and *m*-CPBA as possible oxidants and $C_2H_5OH$, $CH_2Cl_2$, and $CH_3CN$ as possible solvents, the specific combination of $H_2O_2$ and EtOH is found to give the best results for **1** irrespective of the nature of the alkene substrates (Table 2). Among the two other tested oxidants, TBHP and *m*-CPBA, TBHP is found to be relatively better than *m*-CPBA for **1**. The poor solubility of *m*-CPBA in $CH_2Cl_2$ is possibly the reason for the low conversion in all cases. Isomer **2** in general exhibits poor catalytic activity for all of the chosen substrates. However, unlike **1**, the combination of *m*-CPBA and $CH_3CN$ shows relatively better catalytic performance

**Table 2.** Catalytic Results[a]

| substrate | product | solvent | %conversion(selectivity[b]) | | | | | |
|---|---|---|---|---|---|---|---|---|
| | | | Catalyst 1 | | | Catalyst 2 | | |
| | | | $H_2O_2$ | TBHP | *m*-CPBA | $H_2O_2$ | TBHP | *m*-CPBA |
|  |  | EtOH | 78(100) | 90(87) | 95 (93) | 25 (100) | 0 | 65(88) |
| | | DCM | 36(100) | 27(95) | 0 | 0 | 0 | 0 |
| | | ACN | 50(100) | 70(42) | 20(100) | 0 | 0 | 48(100) |
|  |  | EtOH | 100(100) | 91(90) | 100 (87) | 39 (100) | 0 | 70(42) |
| | | DCM | 28(100) | 29(95) | 0 | 0 | 0 | 0 |
| | | ACN | 59(100) | 63(55) | 34(90) | 18(100) | 0 | 67(100) |
|  |  | EtOH | 95 (100) | 65(100) | 84 (91) | 22 (100) | 0 | 55(49) |
| | | DCM | 21(100) | 17(88) | 0 | 0 | 0 | 0 |
| | | ACN | 36(100) | 55(55) | 13(77) | 0 | 0 | 61(100) |
|  |  | EtOH | 71 (100) | 44(100) | 59 (78) | 18(100) | 0 | 39(56) |
| | | DCM | 19(100) | 27(86) | 0 | 0 | 0 | 0 |
| | | ACN | 35(100) | 43 (39) | 9 (90) | 0 | 0 | 53(100) |
| 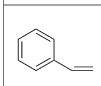 |  | EtOH | 75(100) | 0 | 0 | 10 (15) | 0 | 10(100) |
| | | DCM | 55(100) | 0 | 0 | 0 | 0 | 0 |
| | | ACN | 10(100) | 0 | 0 | 0 | 0 | 15(100) |
|  |  | EtOH | 100(100) | 0 | 0 | 10 (22) | 0 | 10(100) |
| | | DCM | 10(100) | 0 | 0 | 0 | 0 | 0 |
| | | ACN | 10(100) | 0 | 0 | 0 | 0 | 35(100) |
|  |  | EtOH | 86(100) | 0 | 0 | 20 (0) | 0 | 10(100) |
| | | DCM | 5(100) | 0 | 0 | 0 | 0 | 0 |
| | | ACN | 10(100) | 0 | 0 | 0 | 0 | 21(100) |
| 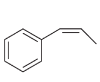 |  | EtOH | 100(100)[c] | 0 | 0 | 8 (22) | 0 | 10(100) |
| | | DCM | 15(100) | 0 | 0 | 0 | 0 | 0 |
| | | ACN | 21(100) | 0 | 0 | 0 | 0 | 43(100) |
| 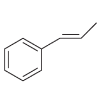 | 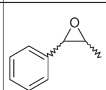 | EtOH | 100(100)[c] | 0 | 0 | 18 (22) | 0 | 10(100) |
| | | DCM | 10(100) | 0 | 0 | 0 | 0 | 0 |
| | | ACN | 19(100) | 0 | 0 | 0 | 0 | 51(100) |
|  |  | EtOH | 100(100) | 90(100) | 100(0)[d] | 0 | 0 | 0 |
| | | DCM | 10(100) | 0 | 0 | 0 | 0 | 0 |
| | | ACN | 10(100) | 0 | 95(0)[d] | 0 | 0 | 95(100) |
|  |  | EtOH | 95(100) | 85(100) | 95(0)[e] | 0 | 0 | 0 |
| | | DCM | 5(100) | 0 | 0 | 0 | 0 | 0 |
| | | ACN | 13(100) | 0 | 90(0)[e] | 0 | 0 | 90(100) |
|  |  | EtOH | 70(100) | 0 | 0 | 5 (100) | 0 | 0 |
| | | DCM | 0 | 0 | 0 | 0 | 0 | 0 |
| | | ACN | 0 | 0 | 0 | 0 | 0 | 0 |
|  |  | EtOH | 100(100) | 70(100) | 88(100) | 0 | 0 | 60 (100) |
| | | DCM | 49(100) | 50(100) | 0 | 0 | 0 | 0 |
| | | ACN | 91 (100) | 80(100) | 50(100) | 0 | 0 | 85(100) |
|  |  | EtOH | 50(100)[f] | 0 | 0 | 0 | 0 | 0 |
| | | DCM | 0 | 0 | 0 | 0 | 0 | 0 |
| | | ACN | 0 | 0 | 0 | 0 | 0 | 0 |
|  |  | EtOH | 43(100)[f] | 0 | 0 | 0 | 0 | 0 |
| | | DCM | 0 | 0 | 0 | 0 | 0 | 0 |
| | | ACN | 0 | 0 | 0 | 0 | 0 | 0 |

[a] Detailed reaction conditions are given in the Experimental Section. Products are characterized by GC. Substrate/catalyst = 200:1 in each case. [b] Selectivity in terms of epoxide formation. [c] See Table S17 for product distribution ratio. [d] Product is 1,2-propanediol, formed with 100% selectivity. [e] Product is 1-chloro-2-hydroxy propane, formed with 100% selectivity. [f] Products are characterized by $^1$H NMR.

for **2** (Table 2). It should be stated that the organic oxidants such as *m*-CPBA and TBHP are known to have limitations particularly because of their low atom efficiency and the formation of organic side-products during the course of the reaction.[2,3e]

Though isomer **1** exhibits excellent catalytic activity in terms of chemoselectivity, percent conversion, and tunability under environmentally benign conditions using $H_2O_2$ as an oxidant and EtOH as a solvent (Table 2),[1d,10] it failed to show any epoxidation reaction with the molecular oxygen ($O_2$) in spite of its larger atom efficiency (50%)[11] than that of $H_2O_2$ (up to 47%). However, oxidation involving molecular oxygen is also known to produce waste from the coreductant, whereas $H_2O_2$ produces $H_2O$ as the only coproduct.[12]

It should be stated that the controlled catalytic experiments in the absence of a substrate reveal that **1** or **2** remains inert toward the oxidation of ethanol under identical experimental conditions (Table 2). Though **1** and **2** behave similarly toward the catalytic epoxidation process in EtOH and *tert*-amyl alcohol (Table 2 and Table S8 in the SI, respectively), catalytic studies have been conducted in an environmentally friendly ethanol solvent.[1d,10]

In general, the performance of catalyst **1** for the epoxidation processes (Table 2) in the presence of an oxidant, $H_2O_2$ in EtOH, is comparable to that reported for other ruthenium based catalysts.[3,4] However, the percent conversion for the substrate stilbene (*cis* and *trans*) using **1** as a catalyst is found to be moderate, though the transformation is totally chemoselective (Table 2). The ruthenium catalyzed epoxidation process is also known to facilitate the cleavage of the C−C bond of epoxides leading to either aldehyde or ketone or alcohol depending on the nature of the substrates,[3,4] as has also been observed with **1** while using oxidant TBHP or *m*-CPBA. However, the epoxidation process using **1** as a catalyst and $H_2O_2$ as an oxidant in EtOH appears to be totally chemoselective irrespective of the percent conversion (Table 2).

The efficiency of catalyst **1** with respect to catalyst loading has also been checked with the specific substrate α-methylstyrene, which shows TON = 1300 even when using a quite low amount (0.01 mol %) of the catalyst (Table S9 in the SI). Upon a further decrease in ruthenium content to 0.001 mol %, the conversion diminishes, but observable activity has also been evidenced (Table S9 in the SI). However, the TON sharply increases from 1300 to 7000

(10) (a) Anastas, P. T.; Warner, J. C. *Green Chemistry: Theory and Practice*; Oxford University Press: New York, 1998; p 30. (b) Capello, C.; Fischer, U.; Hungerbuhler, K. *Green Chem.* **2007**, *9*, 927.

(11) (a) Marky, I. E.; Giles, P. R.; Tsukazaki, M.; Brown, S. M.; Urch, C. J. *Science* **1996**, *274*, 2044. (b) Brink, G.-J.; Arends, I. W. C. E.; Sheldon, R. A. *Science* **2000**, *287*, 1636. (c) Nishiyama, Y.; Nakagawa, Y.; Mizuno, N. *Angew. Chem., Int. Ed.* **2001**, *40*, 3639. (d) Khenkin, A. M.; Shimon, L. J. W.; Neumann, R. *Inorg. Chem.* **2003**, *42*, 3331. (e) Döbler, C.; Mehltretter, G. M.; Sundermeier, U.; Beller, M. *J. Organomet. Chem.* **2001**, *621*, 70. (f) Groves, J. T.; Quinn, R. *J. Am. Chem. Soc.* **1985**, *107*, 5790. (g) Paeng, I. R.; Nakamoto, K. *J. Am. Chem. Soc.* **1990**, *112*, 3289.

(12) (a) Strukul, G. *Catalytic Oxidations with Hydrogen Peroxide as Oxidant*; Kluwer Academic: Dordrecht, The Netherlands, 1992. (b) Jones, C. W. *Applications of Hydrogen Peroxide and Derivatives*; Royal Society of Chemistry: Cambridge, U. K., 1999. (c) Elvers, B.; Hawkins, S.; Ravenscroft, M.; Schulz, G. *Ullmann's Encyclopedia of Industrial Chemistry*, 5th ed.; VCH: New York, 1989; Vol. *A13*, p 443. (d) Kroschwitz, J. I.; Howe-Grant, M. *Kirk-Othmer Encyclopedia of Chemical Technology*, 4th ed.; Wiley: New York, 1995; Vol. *13*, p 961.

upon the subsequent injection of free ligands (0.1 mol % trpy and L each) externally into the reaction system having 0.01 mol % catalyst (Entry 4, Table S9 in the SI). This implies the additional role of free ligands, trpy, and L in the presence of **1** toward the epoxidation process.

The aforementioned observation has prompted us to investigate the individual roles of Ru, trpy, L, mixed trpy/L, and mixed Ru/trpy/L (i.e., the in situ generated metal−ligand(s) based adduct) toward the epoxidation process, and the results are summarized in Table S10 in the SI. It is revealed that under identical reaction conditions ($H_2O_2$ as an oxidant, EtOH as a solvent, α-methylstyrene as a substrate), the use of no Ru or only Ru as $RuCl_3$ or only ligands, trpy/L (Entries 1−3, Table S10 in the SI) is not at all effective in facilitating the epoxidation process. On the other hand, the combinations of Ru (as $RuCl_3$)/trpy and Ru (as $RuCl_3$)/L result in negligible and moderate epoxides, respectively. On the contrary, the use of the combination of Ru (as $RuCl_3$)/trpy/L, i.e., the situation of an *in situ* generated adduct, shows 70% conversion with 90% chemoselective epoxidation (Entry 6, Table S10 in the SI), which is however less than that achieved using the preformed catalyst **1** (Table 2). This in effect implies that the use of a preformed catalyst, isomer **1**, instead of an *in situ* generated catalyst is the better option for the chemoselective epoxidation process.

The aqua complexes, **1′** (corresponds to **1**) and **2′** (corresponds to **2**), have also been synthesized (see the Experimental Section). Complexes **1′** and **2′** exhibit two successive oxidation processes at $E^{\circ}_{298}$ of 0.19 V and 0.41 V and of 0.25 V and 0.56 V at pH 7 versus SCE in $H_2O$, respectively. The potential increases on lowering the pH to 1 at 0.39 V and 0.58 V and at 0.48 V and 0.93 V for **1′** and **2′**, respectively. The successive two oxidation processes are assigned on the basis of earlier reports[4h,9] for the analogous complexes as $\{Ru^{II}-OH_2\} \rightarrow \{Ru^{III}-OH\} + e^- + H^+$ and $\{Ru^{III}-OH\} \rightarrow \{Ru^{IV}=O\} + e^- + H^+$, respectively. The lower oxidation potential of **1′** compared to **2′** implies that the eventual formation of $\{Ru^{IV}=O\}$ species is likely to be more spontaneous in the case of **1′** or **1**. However, we failed to isolate the pure $\{Ru^{IV}=O\}$ species *via* chemical oxidation of the $\{Ru^{II}-H_2O\}$ species using $Ce^{4+}$ salt or $H_2O_2$ as possible oxidants; the initially formed $\{Ru^{IV}=O\}$ species was decomposed to an unidentified material during the workup process. This indeed has precluded conducting any further studies with the $\{Ru^{IV}=O\}$ species; however, detailed studies with the isomeric $\{Ru^{II}-H_2O\}$ species (**1′** and **2′**) are in progress.

Interestingly, under identical experimental conditions, $\{Ru^{II}-Cl\}$ (**1** and **2**) and $\{Ru^{II}-OH_2\}$ (**1′** and **2′**) complexes show similar trends in catalytic properties toward the epoxidation process (Table 2 and Tables S8 and S11 in the SI), which again emphasizes that the specific orientation of L in **1** or **1′** makes the Ru−Cl or Ru−$OH_2$ bond more labile and hence catalytically active compared to the other isomer **2** or **2′**.

The analogous ruthenium−aqua complex incorporating trpy and picolinate ligands in $[Ru^{II}(trpy)(picolinate)(H_2O)]^+$ (the neutral "N" donor of the picolinate ligand was considered *trans* to the $H_2O$ group) was reported to result in nonchemoselective epoxidation processes of styrene derivatives as well as *cis*/*trans*-stilbene using TBHP as an oxidant in a $CH_3CN$ solvent. The effects of other possible isomers (the anionic $O^-$ donor of the picolinate ligand *trans* to the $H_2O$ group) as well as other oxidants and solvents however were not explored.[4i,j]

**Preference of Isomeric Structure on Epoxidation.** The preference for the isomeric structure of **1** over **2** in epoxidation processes (Table 2) can be rationalized on the basis of the following specific considerations: (i) The longer Ru−Cl bond in **1** (2.408(2) Å) compared to that in **2** (2.3813(9) Å) makes it relatively more labile, which in turn facilitates the formation of the active $\{Ru=O\}$ species in the presence of an oxidant, $H_2O_2$. The labile feature of the Ru−Cl bond in $[Ru^{II}(trpy)(L)(Cl)]$ (**1**) has been evidenced by its facile transformation to the single crystals of the corresponding solvate species $[Ru^{II}(trpy)(L)(CH_3CN)](Cl)$ (**1a**, Table 1 and Figure S3 and Table S1 in the SI) while crystallizing **1** from the coordinating acetonitrile solvent over a period of few days. However, the same isomer, **1**, could easily be crystallized from the noncoordinating $CH_2Cl_2$ solvent (Figure 1a and Table 1 and Table S1 in the SI). On the contrary, isomer **2** remains stable in coordinating $CH_3CN$ solvent and thus can be smoothly crystallized without any exchange of "Cl" by the solvent $CH_3CN$ (Figure 1b and Table 1 and Table S1 in the SI; see the Experimental Section). (ii) The addition of $H_2O_2$ in an ethanolic solution of **1** leads to a spontaneous change in color from blue-violet to yellow due to the *in situ* formation of the corresponding ruthenium-oxo species $[Ru^{IV}(trpy)(L)(O)]Cl$ (**3**) as evidenced by its ESI-mass (*m*/*z*, 522.98; calculated mass: 523.03 corresponding to $[Ru^{IV}(trpy)(L)(O)]^+$ ($\mathbf{3}^+$), Figure S4 in the SI) and UV−visible (Figure 4, inset) spectral features.[13] On the subsequent addition of $PPh_3$ to the above solution of **3** in ethanol, the UV−visible spectrum of the oxo-species spontaneously changes to that of the solvate species $[Ru^{II}(trpy)(L)(EtOH)]^+$ (Figure 4, Inset) *via* eq 1.[13] The formation of $Ph_3P=O$ has been evidenced by its characteristic $^{31}P$ NMR peak at 26.25 ppm in $(CD_3)_2SO$.

$$[Ru^{II}(trpy)(L)Cl] \xrightarrow[EtOH]{H_2O_2} [Ru^{IV}(trpy)(L)O]Cl \xrightarrow[-Ph_3P=O]{PPh_3} [Ru^{II}(trpy)(L)(EtOH)]Cl \quad (1)$$

Unlike **1**, under identical reaction conditions, the addition of $H_2O_2$ or *m*-CPBA to the ethanolic solution of **2** yields an unstable oxo species ($\mathbf{4}^+$), which has indeed precluded its further characterization. Consequently, DFT calculations on the optimized ruthenium-oxo species, $[Ru^{IV}(trpy)(L)(O)]^+$ (isomeric $\mathbf{3}^+$ (corresponds to isomer **1**) and $\mathbf{4}^+$ (corresponds to isomer **2**); Figure S5 and Table S12 in the SI) in the triplet, $S = 1$ state [the triplet ($S = 1$) states in $\mathbf{3}^+$ and $\mathbf{4}^+$ are 21.5 and 21.7 kcal/mol, respectively, more stable than the corresponding singlet states], predict that the oxo species, $\mathbf{3}^+$ (corresponding to isomer **1**) is 10.2 kcal/mol more stable than the oxo-counterpart in $\mathbf{4}^+$ (corresponding to isomer **2**). (iii) The NBO analysis on the optimized ruthenium-oxo species ($\mathbf{3}^+$ and $\mathbf{4}^+$) predicts a more negative charge on the oxygen atom of the Ru=O(3) site in $\mathbf{3}^+$ than that in $\mathbf{4}^+$ (NBO/Mulliken charges on the O3 atom of $\mathbf{3}^+$

(13) (a) Dutta, P. K.; Das, S. K. *J. Am. Chem. Soc.* **1997**, *119*, 4311. (b) Taqui Khan, M. M.; Chatterjee, D.; Samad, S. A.; Merchant, R. R. *J. Mol. Catal.* **1990**, *61*, 55. (c) Moyer, B. A.; Sipe, B. K.; Meyer, T. J. *Inorg. Chem.* **1981**, *20*, 1475.

**Scheme 1.** Proposed Reaction Pathway

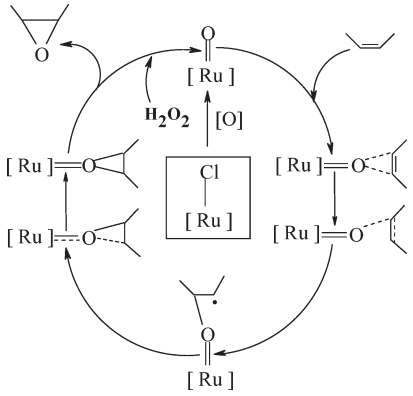


and $\mathbf{4}^+$ are −0.413/−0.480 and −0.318/−0.394, respectively, Table S7 in the SI), while the Ru ion carries an almost similar charge in both cases (NBO/Mulliken charges on the Ru atom are 0.976/1.012 and 1.004/1.015 for $\mathbf{3}^+$ and $\mathbf{4}^+$, respectively, Table S7 in the SI), implying a relatively more polarized Ru−O3 bond in $\mathbf{3}^+$, as has also been reflected in the longer calculated Ru−O(3) bond in $\mathbf{3}^+$ (1.80 Å ($\mathbf{3}^+$) and 1.77 Å ($\mathbf{4}^+$), Table S12 in the SI). (iv) The SOMO of $\mathbf{3}^+$ is primarily dominated by the metal ion (%Ru, L, trpy, O: 53, 23, 4, 20, respectively), while the same in $\mathbf{4}^+$ is dominated by L (%Ru, L, trpy, O: 16, 78, 3, 4, respectively; Tables S13−S14 in the SI), which possibly suggests the less electrophilic character of $\mathbf{4}^+$ as compared to $\mathbf{3}^+$. Thus, the collective effects of relatively better stability and greater electrophilicity of the oxo species in $\mathbf{3}^+$ (corresponding to isomer **1**) in combination with greater polarizability of the longer Ru−O(3) bond in $\mathbf{3}^+$ as compared to $\mathbf{4}^+$ (corresponding to isomer **2**) make it a better active catalyst toward the epoxidation processes in Table 2.

**Mechanistic Outlook.** Metal catalyzed epoxidation of alkenes is known to proceed through the formation of an active metal-oxo species *via* the mediation of a suitable oxidant followed by interaction of the metal bound oxo group with the olefinic double bond leading to an eventual oxo-transfer process, as shown in Scheme 1.[4,5]

In order to ascertain the nature of the active species, either {$Ru^{IV}$=O} or {$Ru^{III}$−OH}, during the catalytic epoxidation process by **1**, the conversion of α-methylstyrene to α-methylstyrene oxide has been tested in the presence of specific hydroxyl radical scavenger N,N′-dimethylthiourea (DMTU).[14] The observed high conversion (91%) of α-methylstyrene to α-methylstyrene oxide even in the presence of a hydroxyl radical scavenger (DMTU; entry no. 2, Table 3) confirms the involvement of {$Ru^{IV}$=O} as the active species. The relatively lower conversion of α-methylstyrene to α-methylstyrene oxide (67%) while using a higher concentration of DMTU (1:5 ratio of **1** and DMTU, entry no. 3, Table 3) could be attributed to the radical mechanism of the reaction (see later).

**Table 3.** Effect of Various Radical Trapping Agents[a]

| entry | radical scavenger[b] | molar equivalent of radical scavenger[c] | conversion (%) | selectivity[d] (%) |
|---|---|---|---|---|
| 1 | - | - | 100 | 100 |
| 2 | DMTU | 1 | 91 | 100 |
| 3 | DMTU | 5 | 67 | 93 |
| 4 | TEMPO | 50 | 21 | 40 |
| 5 | TEMPO | 100 | 0 | 0 |
| 6 | duroquinone | 100 | 53 | 69 |

[a] Detailed reaction conditions are given in the Experimental Section. Products are characterized by GC. Substrate (α-methylstyrene)/catalyst = 200:1 in each case. [b] DMTU: N,N′-dimethylthiourea. TEMPO: 2,2,6,6-tetramethylpiperidine-1-oxyl. Duroquinone: 2,3,5,6-tetramethyl-*p*-benzoquinone. [c] With respect to catalyst. [d] Selectivity in terms of epoxide formation.

**Scheme 2.** Side-On Mode of Binding of the Alkene with the Metal-Oxo Species[a]

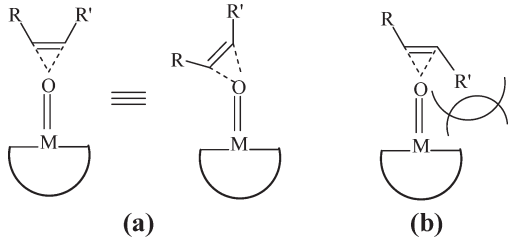


[a] (a) Less hindered approach for *cis*-alkene with respect to (b) *trans*-alkene.

Furthermore, the conversion of sulfide to sulfoxide and/or sulfone by **1** under identical experimental conditions (Table S15 in the SI) also extends additional justification in favor of the {$Ru^{IV}$=O} active species instead of {$Ru^{III}$−OH}.[15]

In metal catalyzed epoxidation reactions, the alkene group is proposed to approach the metal-oxo bond in a side-on fashion[16] (a, Scheme 2), which in effect makes the *cis*-alkene (a) a more active substrate than the corresponding *trans*-alkene primarily due to the steric constraints, as shown in b (Scheme 2).

The transfer of the oxygen atom from the metal-oxo complex to the olefinic double bond has been proposed to proceed *via* five possible intermediates:[16] (a) a concerted transition state, (b) a carbon radical, (c) a carbocation, (d) a $\pi$-radical cation, or (e) a metalaoxetane (Scheme 3).[16f,17]

DFT calculations are performed on the optimized intermediate adduct (**5**) comprised of ruthenium-oxo species in $\mathbf{3}^+$ and styrene as the model substrate considering the convenient side-on approach (Scheme 4, Figure S6, Table S16 in the SI).

The asymmetric side-on approach of the O3 atom of the Ru=O(3) bond in **3** to the incoming alkene function results in intermediate **5**. The calculated $C_\alpha-C_\beta$ and $C_\beta$−O(3) distances of 1.5 and 1.481 Å, respectively, in the optimized structure of **5** imply $sp^2$ and $sp^3$ characters of $C_\alpha$ and $C_\beta$, respectively. Consequently, the calculated Ru−O3 distance in **5** increases to 1.967 Å with respect to

(14) (a) Douglas, E.; Paull, M. D.; Blair, A.; Keagy, M. D.; Eric, J.; Kron, B. S.; Benson, R.; Wilcox, M. D. *J. Surg. Res.* **1989**, *46*, 333. (b) Bunda, S.; Kaviani, N.; Hinek, A. *J. Biol. Chem.* **2005**, *280*, 2341.

(15) (a) Acquaye, J. H.; Muller, J. G.; Takeuchi, K. J. *Inorg. Chem.* **1993**, *32*, 160. (b) Lai, S.; Lepage, C. J.; Lee, D. G. *Inorg. Chem.* **2002**, *41*, 1954. (c) Hamelin, O.; Ménage, S.; Charnay, F.; Chavarot, V; Pierre, J.-L.; Pécaut, J.; Fontecave, M. *Inorg. Chem.* **2008**, *47*, 6413. (d) Chavarot, M.; Ménage, S.; Hamelin, O.; Charnay, F.; Pécaut, J.; Fontecave, M. *Inorg. Chem.* **2003**, *42*, 4810.

(16) (a) Groves, J. T.; Kruper, W. J. *J. Am. Chem. Soc.* **1979**, *101*, 7613. (b) Groves, J. T.; Meyers, R. S. *J. Am. Chem. Soc.* **1983**, *105*, 5786. (c) Jørgensen, K. A. *Chem. Rev.* **1989**, *89*, 431. (d) Meunier, B. *Chem. Rev.* **1992**, *92*, 1411. (e) Jørgensen, K. A.; Schiøtt, B. *Chem. Rev.* **1990**, *90*, 1483. (f) Ostovic, D.; Bruice, T. C. *Acc. Chem. Res.* **1992**, *25*, 314.

(17) Fung, W.-H.; Yu, W.-Y.; Che, C.-M. *J. Org. Chem.* **1998**, *63*, 7715.

**Scheme 3.** Proposed Intermediates for Oxygen Atom Transfer from Metal-Oxo Species to Alkene

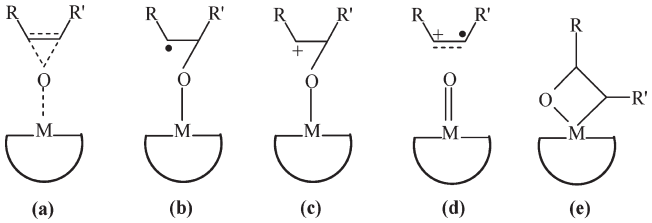


**Scheme 4.** Formation of Epoxide through Radical Pathway

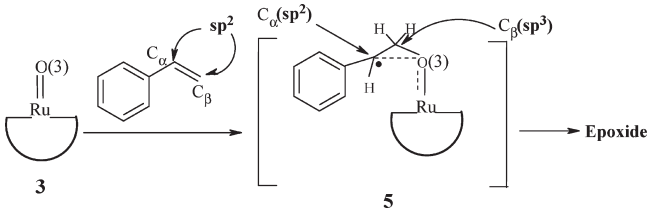


the calculated $Ru^{IV}$=O bond distance of 1.799 Å in $\mathbf{3}^+$, which indeed suggests the single bond character of Ru−O(3) in **5**.[4k] Spin density calculations on **5** predict the spin density of 0.73 on $C_\alpha$, revealing its radical feature (Table S7 in the SI). The calculated NBO and Mulliken charges on Ru in **5**, 0.96 and 0.97, respectively, are close to those calculated for the starting $\mathbf{3}^+$, suggesting the same +4 charge on Ru in both $\mathbf{3}^+$ and **5** (Table S7 in the SI). All of these collectively suggest that the concept of the radical mechanism is also functional in the present case, as has been proposed recently in Ru-catalyzed epoxidation.[4k]

In accordance with the DFT proposed radical intermediate step, b in Scheme 3, the epoxidation of *cis*- or *trans*-β-methylstyrene by **1** results in a mixture of *cis*- and *trans*-β-methylstyrene oxide (Table S17 in the SI) due to isomerization during the lifetime of the intermediate radical state, **5** in Scheme 4.[3p,4h,5g] The formation of *trans*-β-methylstyrene oxide as the major product in each case can be attributed to its thermodynamic stability.[3p,4h,5g]

Moreover, in the presence of free radical scavengers, TEMPO (2,2,6,6-tetramethylpiperidine-1-oxyl) or duroquinone (2,3,5,6-tetramethyl-p-benzoquinone), the conversion as well as chemoselectivity (Table 3) of the reaction, α-methylstyrene to α-methylstyrene oxide, diminish to a large extent, which also clearly justifies the proposed radical mechanism (entry nos. 4−6, Table 3).[5g]

## Conclusion

The following are the salient features of the present work:

- Though preformed ruthenium-aqua complexes with selective coligands[4h,i] or in situ generated ruthenium-solvate species from the preformed coordinatively saturated ruthenium complexes in a bis-tridentate ligand environment[4a,5d−5f] have been established to be suitable molecular frameworks for the catalytic epoxidation process, the present report demonstrates that the preformed synthetically simple {Ru−Cl} species, as in [Ru(trpy)(L)(Cl)] (**1**), can also be a convenient precatalyst for the chemoselective epoxidation process.
- The effect of isomeric structural features of [Ru(trpy)-(L)(Cl)] in **1** and **2** has been reflected in their relevant metal−ligand bond parameters, and consequently **1** and **2** have shown some differences in their spectral and redox processes on the basis of their electronic structural features, as has also been supported by the DFT calculations.
- Remarkably, the limited differences in electronic structural features in isomeric **1** and **2** have been reflected significantly in their catalytic performances toward the epoxidation of olefinic functionalities. Isomer **1** has been established to be an excellent precatalyst for the chemoselective epoxidation of a wide variety of olefins with low catalyst loading under the environmentally benign reaction conditions using $H_2O_2$ as the oxidant and EtOH as the solvent. On the contrary, under identical reaction conditions, isomer **2** is almost inactive and shows some activity only in $CH_3CN$ solvent in the presence of *m*-CPBA as the oxidant (Table 2).
- The experimental and DFT calculations suggest that the greater lability of the {Ru−Cl} bond in isomer **1** than that in **2** and better stability and higher electrophilicity of the active ruthenium-oxo species, [Ru-(trpy)(L)(O)]$^+$, in $\mathbf{3}^+$ (corresponding to the precatalyst **1**) as compared to the isomeric oxo-species $\mathbf{4}^+$ (corresponding to the precatalyst **2**) are the primary contributing factors toward the superior performance of **1** for the epoxidation process.
- The controlled experiments in combination with DFT results establish that the epoxidation reaction proceeds via the involvement of {$Ru^{IV}$=O} active species through a radical pathway, as shown in Scheme 1.

## Experimental Section

**Materials.** The precursor complex Ru(trpy)$Cl_3$ (trpy = 2,2′:6′,2″-terpyridine) was prepared according to literature procedures.[18a] The ligand quinaldic acid (HL) and other reagents and chemicals were obtained from Aldrich and used as received. Solvents were dried by following the standard procedures,[18b] distilled under nitrogen, and used immediately. High purity deionized water used for the electrochemistry experiments of the aqua species (**1′** and **2′**) was obtained by passing distilled water through a nanopure Mili-Q water purification system. For spectroscopic and electrochemical studies, HPLC-grade solvents were used.

**Instrumentation.** $^1H/^{31}P$ NMR spectra were recorded on a 300 MHz Varian spectrometer. IR and UV−vis spectra were recorded using Thermo Nicolet 320 and Perkin-Elmer Lambda 950 spectrophotometers, respectively. ESI-Mass spectra were recorded using a micromass Q-TOF mass spectrometer. Cyclic voltammetric studies were carried out using a PAR model 273A electrochemistry system. Platinum wire working and auxiliary electrodes and an aqueous SCE were used in a three-electrode configuration. The supporting electrolyte was 0.1 M [$NEt_4$][$ClO_4$] ($NaClO_4$ in case of **1′** and **2′**), and the solute concentration was $\sim 10^{-3}$ M. The half-wave potential $E_{298}°$ was set equal to $0.5(E_{pa} + E_{pc})$, where $E_{pa}$ and $E_{pc}$ are the anodic and cathodic cyclic voltammetric peak potentials, respectively. Elemental analyses were carried out on a Perkin-Elmer 240C elemental analyzer. The catalytic reactions were monitored using gas chromatographic techniques with an FID detector (Shimadzu GC-2014 gas chromatograph) using a capillary column (112−2562 CY-CLODEXB, from J&W Scientific, length 60 m, inner diameter 0.25 mm, film 0.25 μm).

**General Procedure for Catalytic Epoxidation Study.** In a typical reaction, the catalyst (0.025 mmol) in 3 mL of solvent (EtOH or *tert*-amyl alcohol or $CH_2Cl_2$ or $CH_3CN$) was placed in a 25 mL Schlenk tube and stirred for 10 min at 298 K. The respective olefins (0.5 mmol) and dodecane (GC internal standard) were then added into the catalyst solution under stirring conditions. The oxidant (3 equiv of 30% $H_2O_2$ or 1.5 equiv of TBHP or 1.2 equiv of 50% *m*-CPBA in 3 mL of respective solvents) was added over a period of 8 h through a syringe pump. The percent yield and percent conversion were determined using the GC technique using respective standard product samples or using $^1$H NMR.

**Crystallography.** Single crystals of **1** and **1a/2** were grown by slow evaporations of their dichloromethane and 1:1 acetonitrile−toluene solutions, respectively. X-ray data were collected using an OXFORD XCALIBUR-S CCD single-crystal X-ray diffractometer. The structures were solved and refined using full matrix least-squares techniques on $F^2$ using the SHELX-97 program.[19] The absorption corrections were done using multiscan (SHELXTL program package), and all data were corrected for Lorentz polarization effects. Hydrogen atoms were included in the refinement process as per the riding model. Selected crystallographic parameters are given in Table 1. The hydrogen atoms associated with the crystallized water and disordered acetonitrile molecules in **1a** could not be located. The asymmetric unit of **1a** contains two crystallographically independent molecules.

**Computational Details.** Full geometry optimizations were carried out at the (R)B3LYP and (U)B3LYP levels[20,21] for **1** and **2** and for $\mathbf{3}^+$, $\mathbf{4}^+$, and **5**, respectively, using the density functional theory method with Gaussian 03 (revision C.02).[22] All elements except ruthenium were assigned the 6-31G(d) basis set. The LanL2DZ basis set with the effective core potential was employed for the ruthenium atom.[23,24] Vertical electronic excitations based on B3LYP optimized geometries were computed for the time-dependent density functional theory (TD-DFT) formalism[25] in acetonitrile using the polarizable continuum model (PCM) of Tomasi and co-workers; specifically, the conductor like PCM (CPCM) in conjugation with the united atom topological model (using UAO radii, implemented in Gaussian 03) was applied.[26−28] GaussSum[29] was used to calculate the fractional contributions of various groups to each molecular orbital. No symmetry constraints were imposed during structural optimizations, and the nature of the optimized structures and energy minima were defined by subsequent frequency calculations. Natural bond orbital analyses were performed using the NBO 3.1 module of Gaussian 03 on optimized geometry.[30] All of the calculated structures were visualized with ChemCraft.[31]

**Synthesis of Isomeric Complexes [Ru(trpy)(L)Cl] (1 and 2).** A total of 100 mg (0.23 mmol) of $Ru(trpy)Cl_3$, 55 mg (0.32 mmol) of quinaldic acid, and $NEt_3$ (1.2 mL, 1.0 mmol) were taken in 15 mL of ethanol. The mixture was heated to reflux for 6 h under a dinitrogen atmosphere. The initial brown color gradually changed to violet, and the solvent of the reaction mixture was evaporated to dryness under reduced pressure. The violet solid thus obtained was dissolved in a minimum volume of $CH_2Cl_2$ and purified by using a neutral alumina column. The blue-violet solution corresponding to isomer **1** was eluted first with $CH_2Cl_2-CH_3OH$ (20:1) followed by the red-violet solution of the isomer **2** with a $CH_2Cl_2-CH_3OH$ (10:1) mixture. On removal of the solvent under reduced pressure, the pure isomeric complexes **1** and **2** were obtained in the solid state.

Complex **1**: Yield, 43 mg (35%). Anal. Calcd for $C_{25}H_{17}N_4ClO_2Ru$ (M.W. 542.01). Found: C, 55.35 (55.15); H, 3.16 (3.08); N, 10.33 (10.42%). $\lambda$ [nm] ($\varepsilon$[$M^{-1}$ $cm^{-1}$]) in acetonitrile: 559 (8477), 417 (7330), 324 (29 859), 312 (27 489), 278 (26 117), 267 (sh), 239 (68 065). ESI-MS (*m*/*z*): 543.85 (**1**), 507.03 (**1**−Cl). $^1$H NMR in $(CD_3)_2SO$ [$\delta$/ppm(*J*/Hz)]: 10.2 (d, 8.8, 1H), 8.7 (d, 8.4, 1H), 8.6 (m, 4H), 8.3 (t, 5.5, 5.1, 1H), 8.1 (d, 8.4, 1H), 7.9 (m, 7H), 7.4 (m, 2H).

Complex **2**: Yield, 37 mg (30%). Anal. Calcd for $C_{25}H_{17}N_4ClO_2Ru$ (M.W. 542.01). Found: C, 55.35 (55.27); H, 3.16 (3.10); N, 10.33 (10.58%). $\lambda$ [nm] ($\varepsilon$[$M^{-1}$ $cm^{-1}$]) in acetonitrile: 533 (14 710), 378 (11 407), 318 (52 359), 310 (sh), 278 (42 199), 239 (111 575). ESI-MS (*m*/*z*): 543.91 (**2**), 507.01 (**2**−Cl). $^1$H NMR in $(CD_3)_2SO$ [$\delta$/ppm (*J*/Hz)]: 8.73 (d, 8.1, 1H), 8.6 (m, 2H), 8.35 (m, 2H), 8.27 (d, 8.1, 1H), 8.16 (d, 8.4, 1H), 7.93 (m, 4H), 7.81 (d, 7.5, 1H), 7.55 (m, 2H), 7.36 (t, 7.5, 7.8, 1H), 7.13 (t, 7.5, 7.5, 1H), 6.44 (d, 8.8,1H).

**Synthesis of Isomeric [Ru(trpy)(L)($H_2O$)]$ClO_4$ (1′) and (2′).** Aqua complexes, **1′** and **2′**, were prepared by adopting the literature reported procedure[9] starting from 50 mg of precursor chloro complexes **1** and **2**, respectively.

Complex **1′**: Yield, 60 mg (52%). Anal. Calcd for $C_{25}H_{19}N_4ClO_7Ru$ (M.W. 624.10). Found: C, 48.08 (47.91); H, 3.07 (3.00); N, 8.98 (8.85%). Molar conductivity [$\Lambda_M$ ($\Omega^{-1}$ $cm^2$ $M^{-1}$)] in dichloromethane = 110. $\lambda$ [nm] ($\varepsilon$[$M^{-1}$ $cm^{-1}$]) in dichloromethane: 497 (3910), 371 (sh), 314 (13 350), 275 (15 110), 241 (37 480). ESI-MS (*m*/*z*): 525.03 (**1′**-$ClO_4$; calcd 525.05), 507.01 (**1′**-$ClO_4-H_2O$; calcd 507.04). $^1$H NMR in $(CD_3)_2CO$ [$\delta$/ppm(*J*/Hz)]: 9.52 (d, 9.9, 1H), 8.85 (d, 10.4, 1H), 8.39 (m, 2H), 8.2 (m, 3H), 8.06 (t, 8.4, 8.6, 2H), 7.98 (t, 8.5, 8.6, 2H), 7.8 (m, 3H), 7.58 (m, 3H)

Complex **2′**: Yield, 65 mg (57%). Anal. Calcd for $C_{25}H_{19}N_4ClO_7Ru$ (M.W. 624.10). Found: C, 48.08(47.99); H, 3.07(2.95); N, 8.98(9.16%). Molar Conductivity [$\Lambda_M$ ($\Omega^{-1}$ $cm^2$ $M^{-1}$)] in dichloromethane = 100. $\lambda$[nm] ($\varepsilon$[$M^{-1}$ $cm^{-1}$]) in dichloromethane: 477 (4480), 374 (sh), 315 (15 330), 274 (15 380),

(18) (a) Sullivan, B. P.; Calvert, J. M.; Meyer, T. J. *Inorg. Chem.* **1980**, *19*, 1404. (b) Perrin, D. D.; Armarego, W. L. F.; Perrin, D. R. *Purification of Laboratory Chemicals*, 2nd ed.; Pergamon: New York, 1980.
(19) Sheldrick, G. M. *SHELX-97*; University of Göttingen: Göttingen, Germany, 1997.
(20) Becke, A. D. *J. Chem. Phys.* **1993**, *98*, 5648.
(21) Lee, C.; Yang, W.; Parr, R. G. *Phys. Rev. B* **1998**, *37*, 785.
(22) Frisch, M. J.; Trucks, G. W.; Schlegel, H. B.; Scuseria, G. E.; Robb, M. A.; Cheeseman, J. R.; Montgomery, J. A.; Vreven, T., Jr.; Kudin, K. N.; Burant, J. C.; Millam, J. M.; Iyengar, S. S.; Tomasi, J.; Barone, V.; Mennucci, B.; Cossi, M.; Scalmani, G.; Rega, N.; Petersson, G. A.; Nakatsuji, H.; Hada, M.; Ehara, M.; Toyota, K.; Fukuda, R.; Hasegawa, J.; Ishida, M.; Nakajima, T.; Honda, Y.; Kitao, O.; Nakai, H.; Klene, M.; Li, X.; Knox, J. E.; Hratchian, H. P.; Cross, J. B.; Adamo, C.; Jaramillo, J.; Gomperts, R.; Stratmann, R. E.; Yazyev, O.; Austin, A. J.; Cammi, R.; Pomelli, C.; Ochterski, J. W.; Ayala, P. Y.; Morokuma, K.; Voth, G. A.; Salvador, P.; Dannenberg, J. J.; Zakrzewski, V. G.; Dapprich, S.; Daniels, A. D.; Strain, M. C.; Farkas, O.; Malick, D. K.; Rabuck, A. D.; Raghavachari, K.; Foresman, J. B.; Ortiz, J. V.; Cui, Q.; Baboul, A. G.; Clifford, S.; Cioslowski, J.; Stefanov, B. B.; Liu, G.; Liashenko, A.; Piskorz, P.; Komaromi, I.; Martin, R. L.; Fox, D. J.; Keith, T.; Al-Laham, M. A.; Peng, C. Y.; Nanayakkara, A.; Challacombe, M.; Gill, P. M. W.; Johnson, B.; Chen, W.; Wong, M. W.; Gonzalez, C.; Pople, J. A. *Gaussian 03*, Revision C.02; Gaussian, Inc.: Wallingford, CT, 2004.
(23) Dunning, T. H., Jr.; Hay, P. J. In *Modern Theoretical Chemistry*; Schaefer, H. F., III, Ed.; Plenum: New York, 1976; p 1.
(24) Hay, P. J.; Wadt, W. R. *J. Chem. Phys.* **1985**, *82*, 299.
(25) (a) Bauernschmitt, R.; Ahlrichs, R. *Chem. Phys. Lett.* **1996**, *256*, 454. (b) Stratmann, R. E.; Scuseria, G. E.; Frisch, M. J. *J. Chem. Phys.* **1998**, *109*, 8218. (c) Casida, M. E.; Jamorski, C.; Casida, K. C.; Salahub, D. R. *J. Chem. Phys.* **1998**, *108*, 4439.
(26) Miertus, S.; Scrocco, E.; Tomasi, J. *Chem. Phys.* **1981**, *55*, 117.
(27) Cossi, M.; Barone, V.; Cammi, R.; Tomasi, J. *Chem. Phys. Lett.* **1996**, *255*, 327.
(28) Barone, V.; Cossi, M. *J. Chem. Phys. A* **1998**, *102*, 1995.
(29) (a) O'Boyle, N. M. *GaussSum 2.1*, 2007. Available at http://gausssum.sf.net (accessed Jan 2011). (b) O'Boyle, N. M.; Tenderholt, A. L.; Langner, K. M. *J. Comput. Chem.* **2008**, *29*, 839.
(30) (a) Glendening, E. D.; Reed, A. E.; Carpenter, J. E.; Weinhold, F. *NBO*, version 3.1; Theoretical Chemistry Institute, University of Wisconsin: Madison, WI, 2001. (b) Reed, A. E.; Weinhold, F. *J. Chem. Phys.* **1985**, *83*, 1736. (c) Reed, A. E.; Curtiss, L. A.; Weinhold, F. *Chem. Rev.* **1988**, *88*, 899. (d) Weinhold, F. In *Encyclopedia of Computational Chemistry*; Schleyer, P. v. R., Ed.; Wiley: New York, 1998; p 1792.
(31) Zhurko, D. A.; Zhurko, G. A. *ChemCraft 1.5*; Plimus: San Diego, CA. http://www.chemcraftprog.com (accessed Jan 2011).

241 (39 730). ESI-MS ($m/z$): 507.03 (**2′**-$ClO_4-H_2O$; calcd 507.04). $^1$H NMR in $(CD_3)_2CO$ [$\delta$/ppm($J$/Hz)]: 8.83 (d, 8.1, 1H), 8.65 (d, 9.4, 1H), 8.41 (d, 8.4, 1H), 8.32 (d, 8.1, 1H), 8.0 (m, 3H), 7.85 (d, 8.3, 1H), 7.64 (m, 3H), 7.4 (m, 3H), 7.25 (m, 2H), 6.45 (d, 9.5,1H).

**Acknowledgment.** This work is Dedicated to Dr. Sumit Bhaduri on the occasion of his 60th birthday. Financial support received from the Department of Science and Technology (DST) and Council of Scientific and Industrial Research (CSIR) (fellowship to A.D.C. and A.D.), New Delhi, India is gratefully acknowledged. X-ray structural studies were carried out at the National Single Crystal Diffractometer Facility, Indian Institute Technology Bombay. $^1$H NMR experiments were carried out at the Sophisticated Analytical Instrument Facility (SAIF), Indian Institute Technology Bombay. Computational facilities from the Department of Chemistry, IIT Bombay are gratefully acknowledged. The reviewers' comments at the revision stage were very helpful.

**Supporting Information Available:** X-ray crystallographic files in CIF format, bond distances/angles, DFT data set and mass spectra (Figures S1−S6 and Tables S1−S17). This material is available free of charge via the Internet at http://pubs.acs.org.